IEEE Access
Multidisciplinary | Rapid Review | Open Access Journal

Received August 17, 2021, accepted August 27, 2021, date of publication August 30, 2021, date of current version September 8, 2021.

Digital Object Identifier 10.1109/ACCESS.2021.3109171

Concentric Ring Array Synthesis for Low Side Lobes: An Overview and a Tool for Optimizing Ring Radii and Angle of Rotation

YANKI ASLAN, (Member, IEEE), ANTOINE ROEDERER, (Life Fellow, IEEE), AND ALEXANDER YAROVOY, (Fellow, IEEE)

Microwave Sensing, Signals and Systems Group, Department of Microelectronics, Delft University of Technology, 2628 Delft, The Netherlands

Corresponding author: Yanki Aslan (y.aslan@tudelft.nl)

This work was supported in part by Netherlands Organisation for Scientific Research (NWO), and in part by NXP Semiconductors in the Framework of the Partnership Program on Advanced 5G Solutions within the Project titled "Antenna Topologies and Front-end Configurations for Multiple Beam Generation" under Grant 15590.

ABSTRACT A comprehensive review on the approaches for synthesizing low side lobe concentric ring array (CRA) antennas is given. An Iterative Convex Optimization (ICO) based array layout synthesis technique is proposed for peak side-lobe level (PSLL) minimization over a given circular field-of-view in steerable uniform-amplitude concentric ring array (UA-CRA) antennas. For a given number of rings and number of uniformly-distributed elements in each ring, the ICO algorithm optimizes the ring radii and angle of rotation, with possible constraints on the minimum element separation and largest array size. As compared to the existing UA-CRA synthesis techniques, the proposed method presents unique features as it combines the capability of optimization of angle of rotation of the rings and PSLL minimization for multiple elevation scan angles in a computationally-efficient and easy-to-solve procedure. Through numerical design examples, it is demonstrated how the ICO technique can be effectively used (i) to synthesize sparse UA-CRA topologies generating low PSLL steerable beams, and (ii) to assess and improve the PSLL suppression performance of various known optimization algorithms. Based on the UA-CRA topologies synthesized via competitive methods in the recent literature, a new set of improved array topologies are presented.

INDEX TERMS Array synthesis, concentric ring arrays, convex optimization, isophoric arrays, low side-lobe level, sparse arrays.

I. INTRODUCTION

Among the various types of planar arrays, the concentric ring array (CRA) antennas have gained more and more attention in modern communication and sensing systems [1]. A CRA is formed by a combination of several concentric rings with different radii, along which the elements are circularly distributed. Thanks to its appealing geometric symmetry, the CRA provides all-azimuth scanning ability and (almost) invariant azimuth-angle coverage capability [2]. Since decades, the rotationally symmetric beam patterns formed by the CRA antennas have played an essential role in applications within the fields of satellite communications [3], radio-astronomy [4], radar [5], and many others.

The associate editor coordinating the review of this manuscript and approving it for publication was Giorgio Montisci.

For the conventional, equally-excited, uniform CRAs with minimum element separation of half-wavelength, the peak side lobe level (PSLL) converges to around −17.5dB [6], which will not satisfy the requirements of many interference-limited scenarios. Therefore, a large number of CRA synthesis techniques for PSLL reduction was proposed, which includes many different optimization methods with distinct capabilities and limitations.

Among the various types of CRA design methods presented in the literature, the global optimization approaches consist of different modifications of Genetic Algorithm (GA) [5], [7]–[11], Particle Swarm Optimization (PSO) [12]–[14], Differential Evolution (DE) [15], Simulated Annealing (SA) [16], Teaching-Learning-Based-Optimization (TLBO) [17] and Moth Flame Optimization (MFO) [18]. In general, these methods are computationally heavy and not applicable to the relatively large-sized

TABLE 1. A broad list of publications on low-PSLL CRA synthesis algorithms with their main features.

Reference \ Feature	optimization of number of elements	optimization of number of rings	optimization of number of elements in each ring	optimization of ring radii	optimization of angle of rotation of rings	optimization of element excitation weights	minimum element separation control	largest array radius control	optimization for multiple scan angles
[5]	✓	✓	✓	✓	–	–	✓	–	–
[7]	✓	✓	✓	✓	–	–	✓	✓	–
[8]	✓	✓	✓	✓	–	–	✓	✓	–
[9]	–	✓	✓	✓	✓	–	✓	✓	✓
[10]	–	–	–	✓	–	–	✓	✓	–
[11]	–	–	–	✓	–	–	✓	✓	–
[12]	–	–	–	–	–	✓	✓	✓	✓
[13]	–	–	–	✓	–	✓	✓	–	–
[14]	✓	–	✓	–	–	–	✓	✓	–
[15]	✓	–	✓	–	–	–	✓	✓	–
[16]	–	–	✓	✓	–	–	✓	✓	–
[17]	✓	–	✓	–	–	–	✓	✓	–
[18]	✓	–	✓	✓	–	✓	✓	–	–
[19]	✓	✓	✓	✓	–	–	✓	✓	–
[20]	✓	✓	–	–	–	✓	✓	–	–
[21]	–	–	✓	✓	–	–	–	✓	–
[22]	✓	✓	✓	✓	✓	–	✓	✓	–
[23]	–	✓	✓	✓	–	–	✓	✓	–
[24]	✓	–	✓	✓	–	–	✓	✓	–
[25]	–	✓	✓	✓	–	–	–	✓	–
[26]	–	✓	✓	✓	–	–	–	✓	–
[27]	–	✓	✓	✓	–	–	–	✓	–
This work	–	–	–	✓	✓	–	✓	✓	✓

arrays due to the large number of unknowns. The analytical approaches, such as the Weighting Density (WD) method [19]–[21], are much more efficient. However, their implementation is based on simple design specifications which limit the performance of the algorithms in terms of optimality. To relax the computational burden of the global optimization tools, hybrid analytical/global or global/convex-programming techniques were proposed. Some examples combine WD with DE [22], WD with GA [23], and GA with Convex Optimization (CO) [24]. As an appealing alternative to the global and analytical methods, Compressive Sensing (CS) based approaches with a well-balanced performance-complexity trade-off were also widely studied in the literature [25]–[27].

An inclusive list of the existing CRA synthesis techniques for PSLL minimization is given in Table 1 together with a qualitative comparison of their characteristics based on the following 9 key questions:
(Q-1) Is the total number of elements optimized?
(Q-2) Is the total number of rings optimized?
(Q-3) Is the number of elements in each ring optimized?
(Q-4) Is the radius of each ring optimized?
(Q-5) Is the angle of rotation of each ring optimized?
(Q-6) Does the array have amplitude and/or phase tapering (i.e. optimization of excitation weights)?
(Q-7) Is it possible to control the minimum element spacing?
(Q-8) Is it possible to control the maximal array size?
(Q-9) Is beam steering taken into account?

In Table 1, the symbol "✓" is used if the technique proposed in the corresponding reference has the relevant feature, while the dash sign "–" is used otherwise.

It is worth to note that a common assumption in the literature is the uniform distribution of the antenna elements on the same ring, which is done to decrease the total number of optimization parameters. From Table 1, it can be observed that several researchers applied optimization of element excitation amplitudes [12], [13], [20] or phases [18] to suppress the PSLL of CRA antennas. On the other hand, due to its practicality and optimal power efficiency, the uniform-amplitude (i.e. isophoric) concentric ring array (UA-CRA) topology was used much more frequently.

Depending on the technique employed, most of the UA-CRA synthesis techniques listed in Table 1 answer 'yes' to a large subset of the above-mentioned questions (Q-1) - (Q-5) and (Q-7) - (Q-9). However, almost all methods (except for [9], [22]) place the first element in each ring along a horizontal line or use random first element locations on the ring. In other words, the angle of rotation of rings is not optimized, which limits the PSLL suppression capability to some extent. Besides, optimization for multiple scan angles was considered only in [9] for UA-CRA antennas, yet with a multi-objective GA that requires large computational resources and time.

In this paper, a novel Iterative Convex Optimization (ICO) based UA-CRA layout synthesis algorithm is introduced for PSLL minimization. The ICO technique has recently been proposed and successfully applied for the low side lobe pattern synthesis in the case of aperiodic array layouts [28], [29]. However, in its current form, the method is not applicable to the CRA antennas. The main novelty of this work with respect to the above-mentioned previous works is the original formulation of the CRA pattern synthesis problem and optimization constraints to be able to apply the ICO and exploit its benefits as compared to the other existing low-PSLL CRA synthesis algorithms. Thus, the presented work is devoted specifically to the application of ICO to the UA-CRA pattern synthesis.

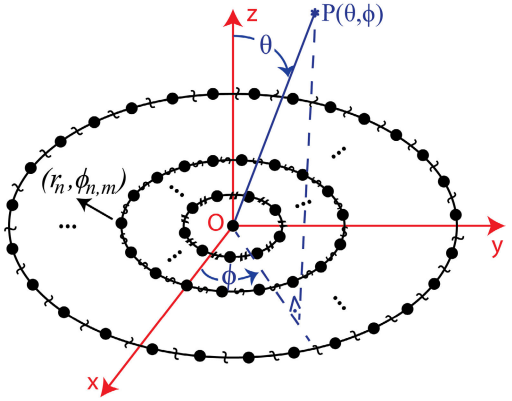

FIGURE 1. Structure of the UA-CRA antenna.

The proposed method is unique in the sense that it combines the capability of optimization of angle of rotation of rings and optimization for multiple scan angles in a computationally-efficient and easy-to-solve procedure. For a given number of rings and number of elements in each ring, the ICO technique optimizes the ring radii and rotation angles.

It is useful to note that in its presented form, the ICO algorithm does not control the number of rings and number of elements in the rings which must be specified at the algorithm input. However, the impact of varying the number of rings and/or elements can be investigated straightforwardly by modifying the initial parameter settings. Such analyses are beyond the scope of this paper. Moreover, the ICO technique can be combined with the existing analytical/global optimization methods to create a hybrid algorithm with extended features and improved optimality in the PSLL. Therefore, it can be directly used as a local optimizer to assess the optimality of different synthesis approaches presented in the literature and to improve their PSLL suppression performance when possible.

The rest of the paper is organized as follows. The ICO-based UA-CRA synthesis algorithm is described in Section II. Several numerical design examples with comparisons to the existing optimization techniques in the recent literature are provided in Section III. The conclusions are presented at the end in Section IV.

II. UA-CRA SYNTHESIS ALGORITHM DESCRIPTION

A comprehensive list of symbols used in this section is provided in Table 2, together with their descriptions. The readers are suggested to refer to this table while following the formulation of the optimization problem explained next.

Let us consider a UA-CRA located in the *xy*-plane with the schematic illustrated in Fig. 1. A center element is placed at the origin, which was shown to be useful for PSLL reduction in the literature [6]. Furthermore, it is assumed that the antenna elements on the same ring are uniformly distributed. Following this approach, the geometric angle of the elements

TABLE 2. Explanation of the symbols used in Section II.

Symbol	Definition
n	index of the ring number, ($n = 1$ is the innermost ring)
m	index of the element number on a ring, ($m = 1$ is the first element while going counterclockwise from $+x$ to $+y$ axis)
N	total number of rings, (the center element at origin does not count as a ring)
M_n	total number of elements in the n-th ring,
r_n	radius of the n-th ring,
$\phi_{n,m}$	geometric angle of the m-th element in the n-th ring,
$x_{n,m}$	x-coordinate of the m-th element in the n-th ring,
$y_{n,m}$	y-coordinate of the m-th element in the n-th ring,
$\epsilon_{n,m}$	position perturbation of the m-th element in the n-th ring along the x-axis,
$\delta_{n,m}$	position perturbation of the m-th element in the n-th ring along the y-axis,
$\boldsymbol{\epsilon}_1$	a vector (of length N) including the position perturbation (along the x-axis) of the first element in each ring
$\boldsymbol{\delta}_1$	a vector (of length N) including the position perturbation (along the x-axis) of the first element in each ring
k	wavenumber, i.e. $2\pi/\lambda$, where λ is the wavelength at the operating frequency
AF	array factor,
(θ, ϕ)	angular coordinates in spherical coordinate system, (θ: elevation angle, ϕ: azimuth angle)
$P(\theta, \phi)$	an arbitrary observation point
(u, v)	coordinate mapping such that $u = \sin\theta\cos\phi$ and $v = \sin\theta\sin\phi$,
(u_s, v_s)	scanning position in the uv-plane for the s-th beam,
$(\boldsymbol{u}, \boldsymbol{v})_{SL,s}$	the set of coordinates in the uv-plane which defines the side lobe region for the s-th beam,
i	iteration number,
$f^{(i,s)}$	the value of a function or variable f at the i-th iteration for the s-th beam
γ	main lobe radius which is about λ/D radians, (i.e. the approximate first null position)
ρ	the maximal side lobe level
μ	upper bound of the position perturbations
$d_{\min}$	minimum inter-element spacing
R	array radius
$\Re$	real part
$\Im$	imaginary part

are defined as

$$\phi_{n,m} = \phi_{n,1} + 2\pi(m-1)/M_n \tag{1}$$

The element positions in Cartesian coordinates are given by

$$x_{n,m} = r_n \cos\phi_{n,m}; \quad y_{n,m} = r_n \sin\phi_{n,m} \tag{2}$$

Let us consider an iterative optimization procedure in which at each iteration i, the position of the first element on each ring n is slightly disturbed in both x- and y-directions by $\epsilon_{n,1}^{(i)}$ and $\delta_{n,1}^{(i)}$, respectively.

$$x_{n,1}^{(i)} = x_{n,1}^{(i-1)} + \epsilon_{n,1}^{(i)}; \quad y_{n,1}^{(i)} = y_{n,1}^{(i-1)} + \delta_{n,1}^{(i)} \tag{3}$$

By putting the optimization variables in a vector form, it can be seen that the total number variables to optimize at each iteration is equal to $2N$.

$$\boldsymbol{\epsilon}_1^{(i)} = \left[\epsilon_{1,1}^{(i)} \ \cdots \ \epsilon_{N,1}^{(i)}\right]; \quad \boldsymbol{\delta}_1^{(i)} = \left[\delta_{1,1}^{(i)} \ \cdots \ \delta_{N,1}^{(i)}\right] \tag{4}$$

The position perturbations at all the remaining elements (except the center element which is not moved) in the CRA are given by

$$\begin{aligned}\epsilon_{n,m}^{(i)} &= \Re\{(\epsilon_{n,1}^{(i)} + j\delta_{n,1}^{(i)})e^{j2\pi(m-1)/M_n}\};\\ \delta_{n,m}^{(i)} &= \Im\{(\epsilon_{n,1}^{(i)} + j\delta_{n,1}^{(i)})e^{j2\pi(m-1)/M_n}\}\end{aligned} \tag{5}$$

The array factor (AF) of the UA-CRA at the i-th iteration is computed as

$$AF^{(i,s)}(u,v) = 1 + \sum_{n=1}^{N}\sum_{m=1}^{M_n}[e^{jk((u-u_s)x_{n,m}^{(i)} + (v-v_s)y_{n,m}^{(i)})}] \tag{6}$$

where u_s and v_s denote the scanning position in the uv-plane for the s-th scanned beam, as indicated in Table 2.

The nonlinear relation between the AF and the element positions makes the optimization of the layout a rather complicated task. One way to linearize the AF expression around the element locations is to assume that the position perturbations at each iteration are sufficiently small (i.e. $|(\epsilon,\delta)_{n,m}^{(i)}| \ll \lambda/2\pi$ [28]). This allows exploiting the first-order Taylor approximation (i.e. $e^{\Delta} = 1 + \Delta$), and ignoring the contribution from the sufficiently small high-order terms $(\epsilon_{n,m}^{(i)})^2$, $(\delta_{n,m}^{(i)})^2$, $(\epsilon_{n,m}^{(i)}\delta_{n,m}^{(i)})$. Furthermore, by applying linearly progressive phase shifts to the array elements for optimal-directivity beam steering towards a particular direction (u_s, v_s), the following approximate relation is derived [29]

$$\begin{aligned}AF_{\epsilon_n,\delta_n}^{(i,s)}(u,v) \approx 1 + \sum_{n=1}^{N}\sum_{m=1}^{M_n}[&e^{jk((u-u_s)x_{n,m}^{(i-1)} + (v-v_s)y_{n,m}^{(i-1)})}\\ &\times (1 + jk(u-u_s)\epsilon_{n,m}^{(i)} + jk(v-v_s)\delta_{n,m}^{(i)})]\end{aligned} \tag{7}$$

Note that in (7), the element positions from the previous iteration $(i-1)$ seen at the exponential terms are known, and the algorithm is initialized with a pre-defined starting layout to be used for the first iteration. For fully-irregular arrays, the impact of the selection of the initial layout on the optimization result in terms of the PSLL was studied in [30] and it was shown that using a low PSLL layout at algorithm initialization could help decrease the number of required iterations, and thus the optimization time, significantly.

To compute the PSLL using (7), the side lobe region for each scanned beam s must be identified. For this aim, a straightforward way is to assume a main lobe radius ($= \gamma$ in the uv-plane), the outside of which defines the region of side lobes.

$$(u,v) \in (\boldsymbol{u},\boldsymbol{v})_{SL,s} \; if \; (u-u_s)^2 + (v-v_s)^2 > \gamma^2 \tag{8}$$

Moreover, there are a number of constraints which might be desired during the array synthesis. The first constraint could be on the maximum allowed size of the array aperture, as shown by

$$r_N \le R \tag{9}$$

When the high-order terms of the sufficiently small-valued optimization variables are omitted for the sake of linearity, the condition in (9) can be approximated by

$$(x_{N,1}^{(i-1)})^2 + 2x_{N,1}^{(i-1)}\epsilon_{N,1}^{(i)} + (y_{N,1}^{(i-1)})^2 + 2y_{N,1}^{(i-1)}\delta_{N,1}^{(i)}) \le R^2 \tag{10}$$

The second constraint could be on the minimum allowed spacing between the array elements due to the physical limitations or the undesirable effects of high mutual coupling levels. A brute-force approach to satisfy this is to check the distance between all the element pairs in the array [29]. For a non-uniform ring radii/rotated CRA layout, a relatively efficient way to ensure a minimal element spacing criterion is: (C-1) to check the distance between element pairs in each ring, and (C-2) to check the distance between one element in a ring with all the elements in the consecutive ring with the larger radius. The condition (C-1) can be expressed as

$$\begin{aligned}&(x_{n,\alpha}^{(i)} - x_{n,\beta}^{(i)})^2 + (y_{n,\alpha}^{(i)} - y_{n,\beta}^{(i)})^2 \ge d_{\min}^2 \text{ holds}\\ &\forall n \in \{1,\ldots,N\},\ \forall(\alpha;\beta) \in \{[1,\ldots,M_n];[1,\ldots,M_n]\}\end{aligned} \tag{11}$$

which can be approximated by

$$\begin{aligned}(\epsilon_{n,\alpha}^{(i)} - \epsilon_{n,\beta}^{(i)})(2x_{n,\alpha}^{(i-1)} - 2x_{n,\beta}^{(i-1)}) + (\delta_{n,\alpha}^{(i)} - \delta_{n,\beta}^{(i)})(2y_{n,\alpha}^{(i-1)}\\ - 2y_{n,\beta}^{(i-1)}) + (x_{n,\alpha}^{(i-1)} - x_{n,\beta}^{(i-1)})^2 + (y_{n,\alpha}^{(i-1)} - y_{n,\beta}^{(i-1)})^2 \ge d_{\min}^2\end{aligned} \tag{12}$$

On the other hand, the condition (C-2) can be expressed as

$$\begin{aligned}&(x_{n,1}^{(i)} - x_{n+1,m}^{(i)})^2 + (y_{n,1}^{(i)} - y_{n+1,m}^{(i)})^2 \ge d_{\min}^2 \text{ holds}\\ &\forall n \in \{1,\ldots,N-1\},\ \forall m \in \{1,\ldots,M_n\}\end{aligned} \tag{13}$$

which can be approximated by

$$\begin{aligned}(\epsilon_{n,1}^{(i)} - \epsilon_{n+1,m}^{(i)})(2x_{n,1}^{(i-1)} - 2x_{n+1,m}^{(i-1)}) + (\delta_{n,1}^{(i)} - \delta_{n+1,m}^{(i)})(2y_{n,1}^{(i-1)}\\ - 2y_{n+1,m}^{(i-1)}) + (x_{n,1}^{(i-1)} - x_{n+1,m}^{(i-1)})^2\\ + (y_{n,1}^{(i-1)} - y_{n+1,m}^{(i-1)})^2 \ge d_{\min}^2\end{aligned} \tag{14}$$

Overall, the ring radii and angle of rotation optimization problem at each iteration of the algorithm for PSLL minimization becomes

$$\min_{\boldsymbol{\epsilon}^{(i)},\boldsymbol{\delta}^{(i)}} \rho^{(i)},\ s.t. \begin{cases} |AF_{\boldsymbol{\epsilon}^{(i)},\boldsymbol{\delta}^{(i)}}^{(i,s)}((\boldsymbol{u},\boldsymbol{v})_{SL,s})| \le \rho^{(i)} \text{ holds } \forall s,\\ |\boldsymbol{\epsilon}_1^{(i)}| \le \mu,\ |\boldsymbol{\delta}_1^{(i)}| \le \mu,\\ (10) \text{ holds},\\ (12) \text{ holds } \forall n \in \{1,\ldots,N\} \text{ and}\\ \quad \forall(\alpha;\beta) \in \{[1,\ldots,M_n];[1,\ldots,M_n]\},\\ (14) \text{ holds } \forall n \in \{1,\ldots,N-1\} \text{ and}\\ \quad \forall m \in \{1,\ldots,M_n\} \end{cases} \tag{15}$$

The optimization procedure in (15) is repeated until convergence on the minimized PSLL, $\rho^{(i)}$ is reached. The formulation results in an Iterative Convex Optimization (ICO) problem, which is a Second-Order Cone Programming (SOCP) problem [31], and it can be efficiently solved

by applying Interior Point Method (IPM) [32] based solvers in free convex optimizers such as CVX [33].

It is also worth to note that to be in line with the literature, the goal function is defined in such a way that the PSLL outside the main lobe in the whole visible space (i.e. $(u^2 + v^2) \leq 1$) is minimized. However, generally, the useful field-of-view or coverage area inside which the beams can be scanned is limited [34], [35]. The area where side-lobes should be controlled, which might extend outside the coverage area, is also generally limited. This allows to push unavoidable side-lobe power of sparse arrays outside the area where side-lobe level matters and thus to improve the in coverage side-lobe level. This appealing feature can be achieved straightforwardly in the proposed algorithm with slight modifications in (8). Moreover, the goal function could be easily modified to minimize the average side-lobe level (ASLL) in the coverage instead of the PSLL, which could also be an important criterion to reduce the interference in some applications [36]. The optimization is performed at a single operation frequency, as commonly applied in the pattern synthesis papers listed in Table 1, and the optimized element positions are given in terms of the wavelength at the corresponding operating frequency. However, it would also be possible to extend the algorithm to multi-frequency optimization for broadband applications, as performed in [37].

III. NUMERICAL DESIGN EXAMPLES

In this section, first, the performance of the proposed algorithm is demonstrated by using the fully-populated, dense, uniform-ring CRA as the benchmark. Next, the proposed ICO algorithm is used to assess the optimality of the recently presented uniform-amplitude CRA synthesis techniques in the literature in terms of the PSLL.

The optimizations in the paper have been performed in MATLAB, using the CVX package with the Self-Dual-Minimization (SeDuMi) solver. The computations have been carried out on an Intel(R) Core(TM) i7-4710HQ 2.5GHz CPU, 16GB RAM computer. Each iteration takes about a minute and the convergence in minimized PSLL is reached in less than 10 minutes in all the cases investigated throughout the paper. The optimization efficiency increases (since the number of iterations decreases) if the initial layout performs close to the final topology in terms of the PSLL (see Section III-B). The uv plane is discretized in steps of 0.01 on a square grid. The upper bound of the position perturbations, μ, is set to 0.08λ in all cases since it has been experimentally observed that this value provides a fast and stable (with no ripples) convergence in the PSLL.

It is worth to note that the impact of mutual coupling is not considered in the examples which study the array factor. However, potentially, the presented ICO algorithm is compatible with the inclusion of mutual coupling via individual embedded element pattern simulations at each iteration. Although it requires additional simulation time and resources, the validity and effectiveness of such a technique was demonstrated in the literature [38]–[40]. Therefore, when the algorithm is used in its full potential (including multiple frequencies and the impact of coupling via iterative full-wave simulations) with more computational requirements, it can deal with any scenario including the design cases with high mutual coupling and large bandwidth.

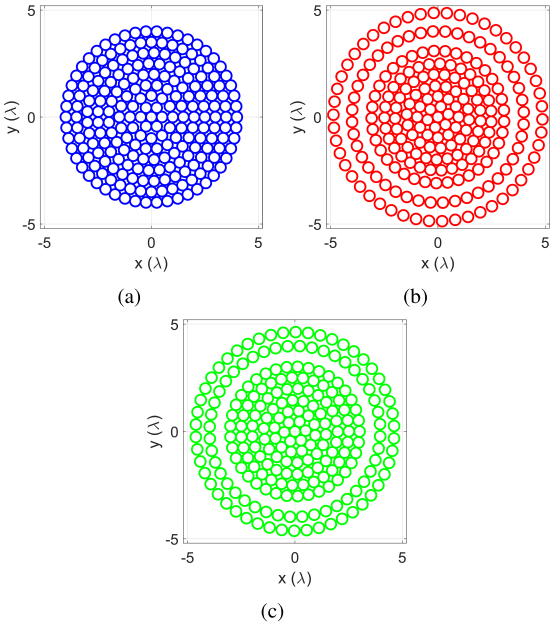

FIGURE 2. 224-element CRA layouts: (a) conventional, (b) optimized via ICO for the broadside beam (i.e. $u_s = v_s = 0$), (c) optimized via ICO for the broadside beam and a scanned beam ($u_s = 0.5$, $v_s = 0$).

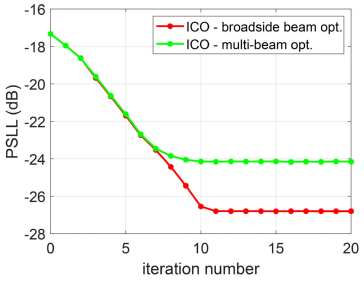

FIGURE 3. PSLL convergence for the 224-element CRA layout optimization in the ICO algorithm.

A. CONVENTIONAL LAYOUT VS ICO ARRAYS

As a reference, the dense 224-element CRA layout with $d_{\min} = 0.5\lambda$, $\phi_{n,1} = 0 \ \forall n \in \{1, \ldots, N = 8\}$ given in Fig. 2(a) is considered. Using this as the initial topology, the proposed ICO procedure is applied. In this part, no restriction is applied on the aperture size R. To define the side lobe region, $\gamma = 0.14$ is used. First, the optimization is performed only for the broadside beam (i.e. $u_s = v_s = 0$) as commonly done in the literature. Then, a multi-beam optimization is performed by considering the broadside beam and a scanned beam ($u_s = 0.5, v_s = 0$) simultaneously. The optimized array topologies are shown in Fig. 2(b) and Fig. 2(c) for the broadside beam optimization and multi-beam

TABLE 3. Geometric configurations of the 224-element layouts given in Fig. 2.

Method	M_1 $r_1(\lambda)$ $\phi_{1,1}(^o)$	M_2 $r_2(\lambda)$ $\phi_{2,1}(^o)$	M_3 $r_3(\lambda)$ $\phi_{3,1}(^o)$	M_4 $r_4(\lambda)$ $\phi_{4,1}(^o)$	M_5 $r_5(\lambda)$ $\phi_{5,1}(^o)$	M_6 $r_6(\lambda)$ $\phi_{6,1}(^o)$	M_7 $r_7(\lambda)$ $\phi_{7,1}(^o)$	M_8 $r_8(\lambda)$ $\phi_{8,1}(^o)$
Conventional	6 0.50 0.00	12 1.00 0.00	18 1.50 0.00	25 2.00 0.00	31 2.50 0.00	37 3.00 0.00	44 3.50 0.00	50 4.00 0.00
ICO -broadside beam opt.-	6 0.50 15.00	12 0.97 30.00	18 1.46 15.00	25 2.00 8.72	31 2.50 6.16	37 3.09 5.46	44 4.01 4.45	50 4.87 4.96
ICO -multi-beam opt.-	6 0.51 3.21	12 0.98 18.21	18 1.47 13.21	25 2.00 0.90	31 2.53 1.90	37 3.03 1.74	44 4.01 3.32	50 4.68 3.41

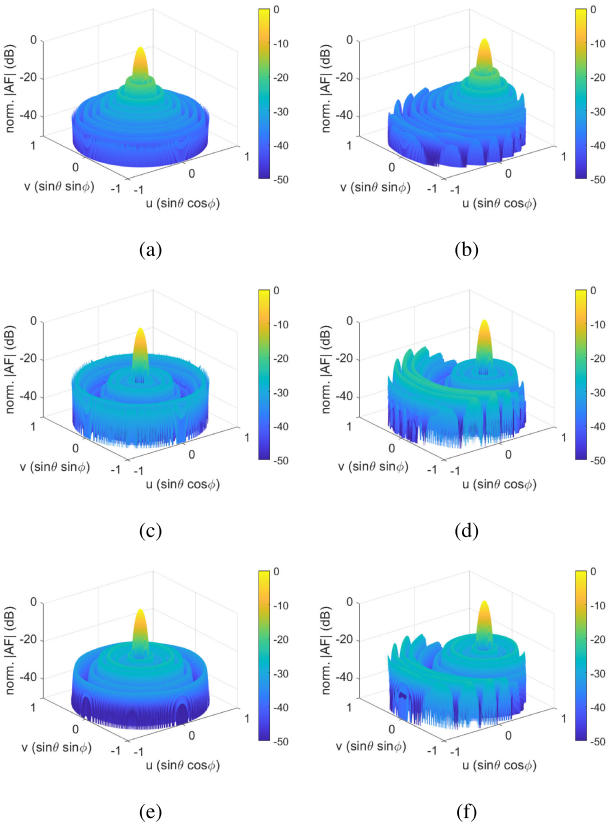

FIGURE 4. The (normalized) array factor of the three CRA layouts given in Fig. 2 for the broadside beam ($u_s = v_s = 0$) and a scanned beam ($u_s = 0.5$, $v_s = 0$): (a) conventional CRA - broadside, (b) conventional CRA - scanned, (c) ICO broadside beam optimized CRA - broadside, (d) ICO broadside beam optimized CRA - scanned, (e) ICO multi-beam optimized CRA - broadside, (f) ICO multi-beam optimized CRA - scanned.

optimization, respectively. Table 3 defines the geometry of the three CRA layouts. The convergence of the PSLL with increasing iteration number ($i = 0$ corresponds to the initial topology) in the proposed ICO algorithm is plotted in Fig. 3. It is seen that the PSLL becomes -26.84dB and -24.10dB in the case of the broadside beam optimization and multi-beam optimization, respectively. Note that the lower PSLL of the broadside beam optimization cannot be preserved when the beam is scanned off-broadside. On the other hand, the PSLL

TABLE 4. Performance comparison summary of the 224-element layouts given in Fig. 2.

Method	$R\,(\lambda)$	D (dBi) ($u_s = 0$, $v_s = 0$)	$PSLL$ (dB) ($u_s = 0$, $v_s = 0$)	D (dBi) ($u_s = 0.5$, $v_s = 0$)	$PSLL$ (dB) ($u_s = 0.5$, $v_s = 0$)
Conventional	4.00	28.37	-17.34	27.68	-17.35
ICO -broadside beam opt.-	4.87	28.79	-26.84	27.58	-21.72
ICO -multi-beam opt.-	4.68	29.02	-24.10	27.59	-24.20

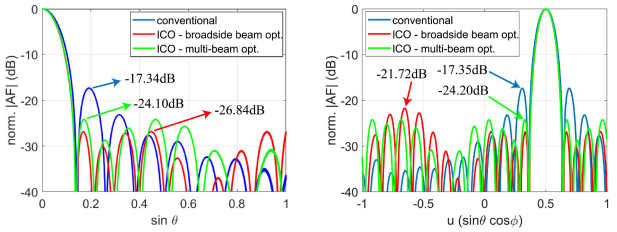

FIGURE 5. Pattern cuts of the array factor plots given in Fig. 4: (a) broadside beam - at different ϕ values (shown with the same color), (b) scanned beam - at $\phi = 0^o$.

in the multi-beam optimization is kept for all the pre-defined scanning angles in the ICO algorithm input.

Fig. 4 provides the *uv*-plane (normalized) array factor of the three CRA layouts given in Fig. 2 for the broadside beam and the scanned beam. For better visualization, Fig. 5(a) shows the pattern cut at different ϕ values (shown with the same color) for the broadside beam, and Fig. 5(b) shows the pattern of the scanned beam at the $\phi = 0^o$ cut. The directivity (D) and PSLL performance of the three arrays for the broadside/scanned beams is summarized in Table 4.

From the simulation results, the following main observations can be made:

(1) Using the same number of rings (and elements in the rings), the PSLL for the broadside beam can be reduced from -17.34dB to -26.84dB just by optimizing the ring radii and angle of rotation. This advantage comes at the expense of a 21.75% increase in the array size. The directivity increases by 0.42dB. It is useful to note here that the PSLL vs array size trade-off can be further investigated by enforcing desired constraints on the input parameter R.

(2) When the beam is scanned to $u_s = 0.5$, $v_s = 0$, the ICO array with broadside beam optimization still provides a lower PSLL than that of the conventional array. However, the PSLL increases by 5.12dB and reaches to -21.72dB. The directivity decreases by 0.1dB as compared to the conventional layout.

(3) The ICO array with multi-beam optimization gives a good trade-off by providing -24.10dB PSLL for the broadside beam and -24.20dB for the scanned beam. Moreover, when compared to the conventional array, the increase in R becomes 17%, the directivity increases by 0.65dB on broadside and decreases only by 0.09dB for the scanned beam.

B. RECENT ALGORITHMS IN THE LITERATURE + ICO

In addition to its use on synthesizing a low PSLL CRA starting from a conventional densely-populated array (or any CRA configuration, in general), the proposed ICO algorithm can be used to assess and when possible, to improve the performance of the recent uniform-amplitude CRA synthesis techniques used for PSLL minimization.

In this section, 4 different study cases using 4 different algorithms are taken as the benchmarks:

(1) Improved Integer Genetic Algorithm (IIGA) [8], which was shown to outperform the commonly used (Modified) Genetic Algorithm ((M)GA) [5], [11].

(2) A Hybrid Approach (HA) combining Continuous Weighting-Density Approximation with a Fine-Adjustment procedure [23].

(3) Quantum Genetic Algorithm based on Hybrid Coding (HCQGA) [7].

(4) A hybrid algorithm (named as DE/WD/VM) combining the Differential Evolutionary (DE) algorithm with Weighting Density (WD) and Vector Mapping (VM) methods [22].

To have a fair comparison, the same values of $N, M_n, R, d_{\min}$ with the reference cases in [7], [8], [22], [23] are used. The optimized topologies in the references are used as the initial topology in the proposed ICO for optimization of the ring radii and angle of rotation for further suppression of the PSLL. The optimizations are performed for the broadside beam only as done in the reference works, yet the ICO algorithm can efficiently handle joint PSLL minimization for multiple beams as well as illustrated in Section III-A. The minimal element separation, $d_{\min} = 0.5\lambda$ in all cases. Considering the array size, the side lobe region is defined by setting $\gamma = 0.15$ in the cases using IIGA and DE/WD/VM and $\gamma = 0.17$ in the cases using HA and HCQGA.

The initial topologies taken from the references (in blue) and the final optimized layouts with the addition of ICO (in red) are given in Fig. 6. The details of the geometry of layouts are listed in Table 5. The convergence of the PSLL in the CO algorithm for the 4 reference study cases is plotted in Fig. 7. Fig. 8 shows the comparison of the (normalized) array factors for the broadside beam in the uv-plane. For better comparison of PSLL, the pattern cuts at multiple ϕ values ($0^o - 360^o$, shown with the same color) are provided in Fig. 9. Finally,

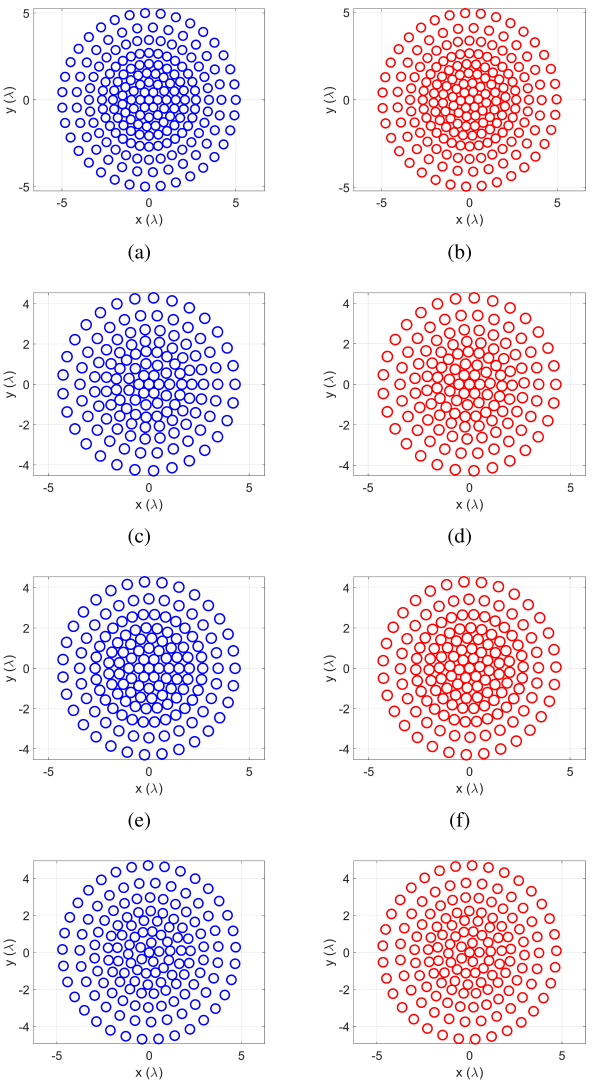

FIGURE 6. Optimized CRA topologies: (a) 190-element IIGA optimized array [8], (b) 190-element IIGA + ICO optimized array, (c) 134-element HA optimized array [23], (d) 134-element HA + ICO optimized array, (e) 148-element HCQGA optimized array [7], (f) 148-element HCQGA + ICO optimized array, (g) 142-element DE/WD/VM optimized array [22], (h) 142-element DE/WD/VM + ICO optimized array.

a summary of the comparative results in terms of array size R, directivity D and $PSLL$ is given in Table 6.

Based on the analyses performed in this section, the following main observations can be made:

(1) Using the optimized topologies in the literature as the initial topology in the proposed ICO algorithm, the topology can be modified to achieve further suppression in the PSLL. For fair comparison, the modification is done in such a way that the number of rings, number of elements in the rings and maximal array radius remain unchanged. The same minimal inter-element distance is kept and the resulting array directivity stays almost the same as well. On the other hand, each ring can be rotated and/or moved along the radial axis. The extent of modification depends on the optimality of the topology given by the reference algorithm.

TABLE 5. Geometric configurations of the optimized CRA antennas given in Fig. 6.

Method	M_1 $r_1(\lambda)$ $\phi_{1,1}(^o)$	M_2 $r_2(\lambda)$ $\phi_{2,1}(^o)$	M_3 $r_3(\lambda)$ $\phi_{3,1}(^o)$	M_4 $r_4(\lambda)$ $\phi_{4,1}(^o)$	M_5 $r_5(\lambda)$ $\phi_{5,1}(^o)$	M_6 $r_6(\lambda)$ $\phi_{6,1}(^o)$	M_7 $r_7(\lambda)$ $\phi_{7,1}(^o)$	M_8 $r_8(\lambda)$ $\phi_{8,1}(^o)$
IIGA [8]	6 0.50 0.00	12 1.01 0.00	19 1.54 0.00	24 2.07 0.00	32 2.70 0.00	32 3.45 0.00	29 4.17 0.00	35 5.00 0.00
IIGA + ICO	6 0.50 5.28	12 0.97 20.28	19 1.52 16.32	24 2.05 4.57	32 2.65 0.21	32 3.38 0.01	29 4.11 12.23	35 4.96 0.31
HA [23]	6 0.50 0.00	11 1.03 0.00	19 1.64 0.00	19 2.14 0.00	23 2.72 0.00	26 3.43 0.00	29 4.30 0.00	-
HA + ICO	6 0.52 0.00	11 1.02 2.72	19 1.61 16.11	19 2.11 17.69	23 2.70 1.50	26 3.42 13.85	29 4.27 12.32	-
HCQGA [7]	6 0.50 0.00	12 1.00 0.00	17 1.50 0.00	23 2.01 0.00	30 2.68 0.00	28 3.45 0.00	31 4.30 0.00	-
HCQGA + ICO	6 0.51 8.26	12 0.98 23.26	17 1.50 9.75	23 2.01 9.94	30 2.67 1.52	28 3.43 0.45	31 4.30 0.79	-
DE/WD/VM [22]	5 0.54 5.72	14 1.14 4.40	15 1.74 3.50	21 2.24 2.21	26 2.97 5.98	27 3.76 4.90	33 4.70 3.46	-
DE/WD/VM + ICO	5 0.53 1.01	14 1.14 2.68	15 1.74 2.98	21 2.24 4.69	26 2.97 11.04	27 3.76 12.94	33 4.70 1.05	-

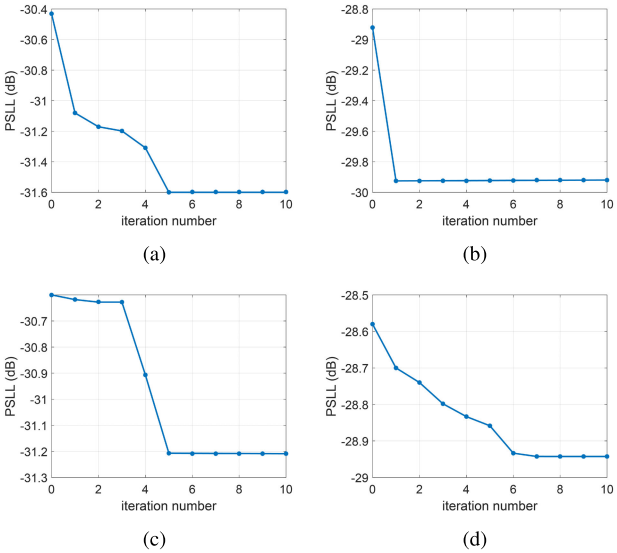

FIGURE 7. PSLL convergence in the ICO algorithm for the initial CRA layout of: (a) 190-element IIGA optimized array [8], (b) 134-element HA-optimized array [23], (c) 148-element HCQGA optimized array [7], (d) 142-element DE/WD/VM optimized array [22].

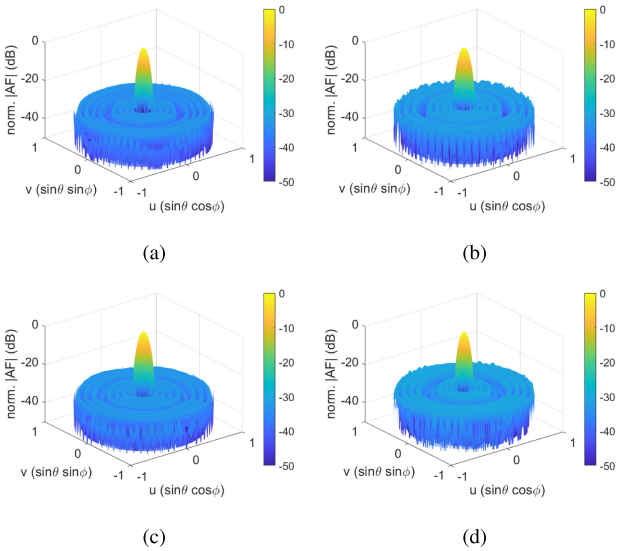

FIGURE 8. The (normalized) array factor of the four ICO-optimized CRA layouts given in Fig. 6 for the broadside beam: (a) 190-element IIGA + ICO, (b) 134-element HA + ICO, (c) 148-element HCQGA + ICO, (d) 142-element DE/WD/VM + ICO.

(2) For the IIGA optimized 190-element array, the addition of ICO brings 1.17dB additional reduction in the PSLL, while the array size decreases by 0.8% and the directivity reduces only by 0.11dB.

(3) For the HA optimized 134-element array, the addition of ICO brings 1.01dB additional reduction in the PSLL and the directivity increases slightly by 0.05dB, while the array size decreases by 0.7%.

(4) For the HCQGA optimized 148-element array, the addition of ICO brings 0.62dB additional reduction in the PSLL, while the array size remains unchanged and the directivity reduces only by 0.05dB.

(5) For the DE/WD/VM optimized 142-element array, the addition of ICO brings only 0.36dB additional reduction in the PSLL, while the array size and directivity remain the same.

(6) In all the cases studied above, the inclusion of ICO improves the overall algorithm performance to some extent. However, among the 4 reference algorithms, the DE/WD/VM algorithm (which is the most resistant to the ICO) appears to be the best in terms of PSLL suppression capability. This is due to the distinctive ability of the algorithm to optimize the angle of rotation of the rings (or $\phi_{n,1}$ for each n), while

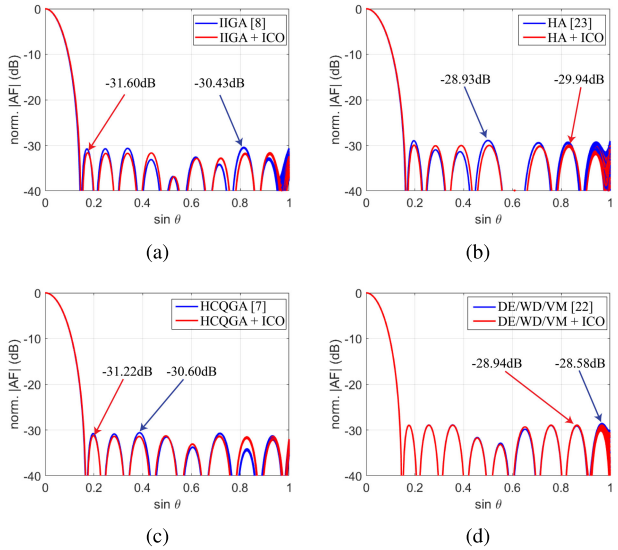

FIGURE 9. Comparison of the array factor at broadside for pattern cuts at different ϕ values (shown with the same color): (a) IIGA [8] vs IIGA + ICO, (b) HA [23] vs HA + ICO, (c) HCQGA [7] vs HCQGA + ICO, (d) DE/WD/VM [22] vs DE/WD/VM + ICO.

TABLE 6. Performance comparison summary of the optimized CRA layouts given in Fig. 6.

Method	R (λ)	D (dBi) ($u_s = 0, v_s = 0$)	$PSLL$ (dB) ($u_s = 0, v_s = 0$)
IIGA [8]	5.00	29.48	-30.43
IIGA + CO	4.96	29.37	-31.60
HA [23]	4.30	28.12	-28.93
HA + CO	4.27	28.17	-29.94
HCQGA [7]	4.30	28.35	-30.60
HCQGA + CO	4.30	28.30	-31.22
DE/WD/VM [22]	4.70	28.80	-28.58
DE/WD/VM + CO	4.70	28.80	-28.94

in IIGA, HA and HCQGA, there is no ring rotation (i.e. $\phi_{n,1} = 0 \ \forall n$).

It is worth to note that the most recent, competitive and relevant UA-CRA synthesis techniques in [7], [8], [22], [23] have been considered in Section III-B, for which the optimized layouts (i.e. element positions) and optimization constraints (i.e. minimum inter-element spacing, maximum array radius) are clearly provided in the corresponding references. Since only the broadside beam is considered in these papers during the optimization, the ICO has been used in the broadside beam optimization mode to have a fair comparison. The feature of optimization for scanned beams has been illustrated in Section III-A by using a conventional dense array as the benchmark. Among the comprehensive list of CRA synthesis techniques provided in Table 1, only [9] and [12] have the feature of optimization for multiple scan angles. In [9], a large number of sub-optimal CRA configurations are obtained by using the Non–dominated Sorting Genetic Algorithm II (NSGA-II). The designer then observes and chooses the best trade-off solution in terms of the PSLL for the broadside beam and the scanned beam. On the other hand, the proposed ICO technique provides the single optimal trade-off solution in a much more efficient way. As the optimized element locations and inter element spacings are not clearly provided in [9], it has not been used as a reference in the quantitative comparisons given in Section III-B. Differently, in [12], the optimization is performed on the excitation amplitudes and phases (not on the ring radii, angle or density). However, due to their practicality and optimal power efficiency, our interest is in the layout-optimized UA-CRAs. Therefore, [12] has not been considered as a relevant reference for the quantitative comparison.

IV. CONCLUSION

An innovative ICO algorithm for the synthesis of UA-CRA antennas has been presented. The method is used to generate low PSLL array topologies for the desired number of rings, number of elements in each ring, minimum distance between the elements and scan angles. The proposed technique provides an efficient way to assess the optimality of the various types of algorithms in the literature. Moreover, it can be straightforwardly combined with the existing algorithms to improve their PSLL suppression performance, when possible. The extent of further reduction in the PSLL depends on the optimality of the initial array layout obtained from the reference algorithm.

The main novelties of this work include (i) a new formulation of the low PSLL UA-CRA synthesis problem to enable the use of numerically efficient convex solvers, (ii) the first-time development of a low-computational-complexity methodology for the optimization of ring radii and rotation angles simultaneously for multiple scanned beams, (iii) a new and fast version of the minimum element separation control in convex programming for CRA architectures, (iv) an original flexible, non-complex, yet effective local optimizer tool compatible with the prior CRA synthesis methods.

The effectiveness of the proposed technique has been demonstrated by using conventional-dense and optimized-sparse CRA topologies from the recent literature as benchmarks. It has been shown that the UA-CRA antennas optimized via ICO exhibit lower PSLL as compared to the benchmarks, with no significant decrease in array directivity. The extent of reduction in PSLL depends on the optimality of the benchmark topology which is used at the algorithm initialization.

The ICO CRA synthesis method is potentially able to (i) suppress the PSLL within a given limited circular field-of-view by pushing the unavoidable side-lobe power of sparse arrays outside the coverage area, (ii) study the impact of varying the number of rings and/or number of elements in each ring, (iii) use stepped excitations for further PSLL reduction at the expense of a decrease in directivity, (iv) use different kind of feeds for each ring for increased design flexibility, (v) include the impact of mutual coupling via individual embedded pattern simulations at each iteration, (vi) adapt to broadband operation with multi-frequency optimization. These aspects are out of the scope of this paper and will be further studied in future works.

REFERENCES

[1] P. Rocca, G. Oliveri, R. J. Mailloux, and A. Massa, "Unconventional phased array architectures and design methodologies—A review," *Proc. IEEE*, vol. 104, no. 3, pp. 544–560, Mar. 2016.

[2] R. J. Mailloux, *Phased Array Antenna Handbook*. Norwood, MA, USA: Artech House, 2017.

[3] O. M. Bucci and S. Perna, "A deterministic two dimensional density taper approach for fast design of uniform amplitude pencil beams arrays," *IEEE Trans. Antennas Propag.*, vol. 59, no. 8, pp. 2852–2861, Jun. 2011.

[4] Y. Chow, "Comparison of some correlation array configurations for radio astronomy," *IEEE Trans. Antennas Propag.*, vol. AP-18, no. 4, pp. 567–569, Jul. 1970.

[5] R. L. Haupt, "Optimized element spacing for low sidelobe concentric ring arrays," *IEEE Trans. Antennas Propag.*, vol. 56, no. 1, pp. 266–268, Jan. 2008.

[6] M. I. Dessouky, H. A. Sharshar, and Y. A. Albagory, "Efficient sidelobe reduction technique for small-sized concentric circular arrays," *Prog. Electromagn. Res.*, vol. 65, pp. 187–200, Jan. 2006.

[7] Q. Guo, Y. Wang, D. Yuan, J. Li, and T. Yu, "Optimization of sparse concentric ring arrays based on multiple constraints," *IEEE Antennas Wireless Propag. Lett.*, vol. 19, no. 5, pp. 781–785, May 2020.

[8] Y. Jiang, S. Zhang, Q. Guo, and M. Li, "Synthesis of uniformly excited concentric ring arrays using the improved integer GA," *IEEE Antennas Wireless Propag. Lett.*, vol. 15, pp. 1124–1127, Oct. 2016.

[9] D. Bianchi, S. Genovesi, and A. Monorchio, "Constrained Pareto optimization of wide band and steerable concentric ring arrays," *IEEE Trans. Antennas Propag.*, vol. 60, no. 7, pp. 3195–3204, Jul. 2012.

[10] K. Chen, Y. Li, and J. Shi, "Optimization of sparse concentric ring arrays for low sidelobe," *Int. J. Antennas Propag.*, vol. 2019, pp. 1–8, Jun. 2019.

[11] K.-S. Chen, Y.-Y. Zhu, X.-L. Ni, and H. Chen, "Low sidelobe sparse concentric ring arrays optimization using modified GA," *Int. J. Antennas Propag.*, vol. 2015, pp. 1–5, May 2015.

[12] A. Reyna and M. A. Panduro, "Design of steerable concentric rings array using rotation properties and evolutionary optimization," in *Proc. 4th EuCAP*, Barcelona, Spain, Apr. 2010, pp. 1–5.

[13] E. I. Elsaidy, M. I. Dessouky, S. Khamis, and Y. A. Albagory, "Concentric circular antenna array synthesis using comprehensive learning particle swarm optimizer," *Prog. Electromagn. Res.*, vol. 29, pp. 1–13, Dec. 2012.

[14] N. Pathak, P. Nanda, and G. K. Mahanti, "Synthesis of thinned multiple concentric circular ring array antennas using particle swarm optimization," *J. Infr., Millim., THz Waves*, vol. 30, no. 7, pp. 709–716, Apr. 2009.

[15] P. Ghosh and S. Das, "Synthesis of thinned planar concentric circular antenna arrays—A differential evolutionary approach," *Prog. Electromagn. Res.*, vol. 29, pp. 63–82, Jan. 2011.

[16] A. Á. Salas-Sánchez, J. A. Rodríguez-González, E. Moreno-Piquero, and F. J. Ares-Pena, "Synthesis of Taylor-like patterns with uniformly excited multi-ring planar antennas," *IEEE Trans. Antennas Propag.*, vol. 62, no. 4, pp. 1589–1595, Apr. 2014.

[17] Z. Luo, X. He, X. Chen, X. Luo, and X. Li, "Synthesis of thinned concentric circular antenna arrays using modified TLBO algorithm," *Int. J. Antennas Propag.*, vol. 2015, pp. 1–9, Jul. 2015.

[18] D. Jamunaa, G. Mahanti, and F. N. Hasoon, "Optimized inter-element arc spacing and ring radius in the synthesis of phase-only reconfigurable concentric circular array antenna using various evolutionary algorithms," *Electromagn.*, vol. 40, no. 2, pp. 104–118, Jan. 2020.

[19] T. A. Milligan, "Space-tapered circular (ring) array," *IEEE Antennas Propag. Mag.*, vol. 46, no. 3, pp. 70–73, Jun. 2004.

[20] M. I. Dessouky, H. A. Sharshar, and Y. A. Albagory, "Optimum normalized-Gaussian tapering window for side lobe reduction in uniform concentric circular arrays," *Prog. Electromagn. Res.*, vol. 69, pp. 35–46, Jan. 2007.

[21] P. Angeletti and G. Toso, "Synthesis of circular and elliptical sparse arrays," *Electron. Lett.*, vol. 47, no. 5, pp. 304–305, 2011.

[22] S. Xie, J. Li, H. Shao, L. Guo, and G. Deng, "A DE/WD/VM hybrid algorithm for multiple constraint synthesis of concentric ring arrays," in *Proc. 50th EuMC*, Utrecht, The Netherlands, Jan. 2021, pp. 65–68.

[23] Q. Guo, C. Chen, and Y. Jiang, "An effective approach for the synthesis of uniform amplitude concentric ring arrays," *IEEE Antennas Wireless Propag. Lett.*, vol. 16, pp. 2558–2561, Jul. 2017.

[24] O. M. Bucci and D. Pinchera, "A generalized hybrid approach for the synthesis of uniform amplitude pencil beam ring-arrays," *IEEE Trans. Antennas Propag.*, vol. 60, no. 1, pp. 174–183, Jan. 2012.

[25] C. Bencivenni, M. V. Ivashina, and R. Maaskant, "Synthesis of circular isophoric sparse arrays by using compressive-sensing," in *Proc. IEEE APS/URSI*, Fajardo, Puerto Rico, Jun. 2016, pp. 761–762.

[26] X. Zhao, Q. Yang, and Y. Zhang, "A hybrid method for the optimal synthesis of 3-D patterns of sparse concentric ring arrays," *IEEE Trans. Antennas Propag.*, vol. 64, no. 2, pp. 515–524, Feb. 2016.

[27] M. Carlin, G. Oliveri, and A. Massa, "Hybrid BCS-deterministic approach for sparse concentric ring isophoric arrays," *IEEE Trans. Antennas Propag.*, vol. 63, no. 1, pp. 378–383, Jan. 2015.

[28] B. Fuchs, A. Skrivervik, and J. R. Mosig, "Synthesis of uniform amplitude focused beam arrays," *IEEE Antennas Wireless Propag. Lett.*, vol. 11, pp. 1178–1181, Oct. 2012.

[29] Y. Aslan, J. Puskely, A. Roederer, and A. Yarovoy, "Multiple beam synthesis of passively cooled 5G planar arrays using convex optimization," *IEEE Trans. Antennas Propag.*, vol. 68, no. 5, pp. 3557–3566, May 2020.

[30] Y. Aslan, J. Puskely, A. Roederer, and A. Yarovoy, "Effect of element number reduction on inter-user interference and chip temperatures in passively-cooled integrated antenna arrays for 5G," in *Proc. 14th EuCAP*, Copenhagen, Denmark, Mar. 2020, pp. 1–4.

[31] F. Alizadeh and D. Goldfarb, "Second-order cone programming," *Math. Program.*, vol. 95, no. 1, pp. 3–51, 2003.

[32] M. S. Lobo, L. Vandenberghe, S. Boyd, and H. Lebret, "Applications of second-order cone programming," *Linear Algebra Appl.*, vol. 284, nos. 1–3, pp. 193–228, Nov. 1998.

[33] M. Grant and S. Boyd. (Mar. 2014). *CVX: MATLAB Software for Disciplined Convex Programming, Version 2.1*. [Online]. Available: http://cvxr.com/cvx

[34] J. Wang, K. Chan, M. Cuchanski, and K. Rao, "Direct radiating array for MEO communication satellite," in *Proc. ANTEM*, Montreal, QC, Canada, Aug. 1996, pp. 579–582.

[35] C. Bencivenni, M. V. Ivashina, R. Maaskant, and J. Wettergren, "Synthesis of maximally sparse arrays using compressive sensing and full-wave analysis for global earth coverage applications," *IEEE Trans. Antennas Propag.*, vol. 64, no. 11, pp. 4872–4877, Nov. 2016.

[36] F. A. Dicandia and S. Genovesi, "Exploitation of triangular lattice arrays for improved spectral efficiency in massive MIMO 5G systems," *IEEE Access*, vol. 9, pp. 17530–17543, Jan. 2021.

[37] L. T. P. Bui, N. Anselmi, T. Isernia, P. Rocca, and A. F. Morabito, "On bandwidth maximization of fixed-geometry arrays through convex programming," *J. Electromagn. Waves Appl.*, vol. 34, no. 5, pp. 581–600, Feb. 2020.

[38] J. I. Echeveste, M. A. G. de Aza, J. Rubio, and C. Craeye, "Gradient-based aperiodic array synthesis of real arrays with uniform amplitude excitation including mutual coupling," *IEEE Trans. Antennas Propag.*, vol. 65, no. 2, pp. 541–551, Feb. 2017.

[39] H. B. Van, S. N. Jha, and C. Craeye, "Fast full-wave synthesis of printed antenna arrays including mutual coupling," *IEEE Trans. Antennas Propag.*, vol. 64, no. 12, pp. 5163–5171, Dec. 2016.

[40] Y. Aslan, M. Candotti, and A. Yarovoy, "Synthesis of multi-beam space-tapered linear arrays with side lobe level minimization in the presence of mutual coupling," in *Proc. 13th EuCAP*, Krakow, Poland, Apr. 2019, pp. 1–5.

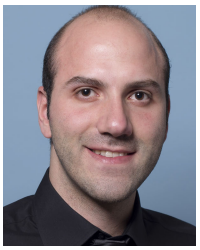

YANKI ASLAN (Member, IEEE) was born in Ankara, Turkey, in 1991. He received the B.Sc. degree with double specialization in communications and microwaves/antennas from the Department of Electrical and Electronic Engineering, Middle East Technical University, Ankara, in 2014, and the M.Sc. and Ph.D. degrees *(cum laude)* in electrical engineering from Delft University of Technology (TU Delft), Delft, The Netherlands, in 2016 and 2020, respectively. Following his postdoctoral research at the Microwave Sensing, Signals and Systems (MS3) Group, TU Delft, where he worked as an Assistant Professor, in April 2021. His current research interests include phased arrays for next-generation communication and sensing systems, array optimization, multibeam antennas, front-end architectures, and beamforming algorithms. He was one of the recipients of the IEEE AP-S Doctoral Research Grant, in 2018, and the EuMA Internship Award, in 2019.

ANTOINE ROEDERER (Life Fellow, IEEE) was born in Paris, France, in 1943. He received the B.S.E.E. degree from the École Supérieure d'Électricite, Paris, in 1964, the M.S.E.E. degree from the University of California at Berkeley, Berkeley, CA, USA, in 1965, the Doctorate degree (Hons.) in electrical engineering from the Universite de Paris VI, Paris, in 1972, and the Honorary Doctorate degree from the Technical University of Delft, Delft, The Netherlands, in 2005.

He was a Radar Antenna Research and Development Engineer with THOMSON-CSF, Bagneux, France, from 1968 to 1973. He joined the European Space Research and Technology Centre, ESRO [now European Space Agency (ESA)], Noordwjik, The Netherlands, in 1973, where he initiated and supervised research and development and project support for space antennas for many years. In 1993, he became the Head of the Electromagnetics Division, ESA. He retired from ESA, in 2008. He is currently a part-time Scientific Advisor with the Technical University of Delft. He has authored or coauthored over 150 articles, several book chapters, and holds 20 patents in the field of antennas. This has included aspects of wideband communications, broadcasting, radar, and satellite antennas, with an emphasis on log-periodics, reflectarrays, multiple-beam reflectors and arrays, and advanced antenna feed networks. His current research interests include innovation and development in the fields of radar and 5G base station antennas. He received numerous awards for his contributions to the field of antennas and the antenna community in Europe. He received the Fulbright Fellowship for his M.S.E.E degree. He has been the Chairman of the EU COST 260 Project on Smart Antennas. He was the Initiator and the Chairman of the Millennium Conference on Antennas and Propagation (AP 2000), Davos, and a precursor of the large EUCAP conferences.

ALEXANDER YAROVOY (Fellow, IEEE) received the Diploma degree (Hons.) in radiophysics and electronics and the Candidate of Sciences in Physics and Mathematics and Doctor of Sciences in Physics and Mathematics degrees in radiophysics from Kharkov State University, Kharkiv, Ukraine, in 1984, 1987, and 1994, respectively.

In 1987, he joined the Department of Radiophysics, Kharkov State University, as a Researcher, where he became a Professor, in 1997. From September 1994 to 1996, he was with the Technical University of Ilmenau, Ilmenau, Germany, as a Visiting Researcher. Since 1999, he has been with Delft University of Technology, Delft, The Netherlands. Since 2009, he has been leading the Chair of the Microwave Sensing, Systems and Signals Group. He has authored or coauthored more than 450 scientific or technical articles, four patents, and 14 book chapters. His main research interests include in high-resolution radar, microwave imaging, and applied electromagnetics (in particular UWB antennas).

Dr. Yarovoy was a recipient of the European Microwave Week Radar Award for the paper that best advances the state-of-the-art in radar technology, in 2001 (together with L. P. Ligthart and P. van Genderen), and in 2012 (together with T. Savelyev). In 2010, together with D. Caratelli, he received the Best Paper Award of the Applied Computational Electromagnetic Society (ACES). He served as the Chair and the TPC Chair for the Fifth European Radar Conference (EuRAD'08), Amsterdam, The Netherlands, and the Secretary of the First European Radar Conference (EuRAD'04), Amsterdam. He also served as the Co-Chair and the TPC Chair for the Xth International Conference on GPR (GPR2004), Delft. From 2008 to 2017, he served as the Director for the European Microwave Association (EuMA). He served as a Guest Editor of five special issues for the IEEE TRANSACTIONS and other journals. Since 2011, he has been an Associate Editor of the *International Journal of Microwave and Wireless Technologies*.